AGU PUBLICATIONS

Geophysical Research Letters

RESEARCH LETTER
10.1002/2015GL067015

Key Points:
- A discrete-domain description of two-phase displacements
- Connection between hysteresis and rugged energy landscapes
- A mechanistic hysteresis model with a unique compartment description

Correspondence to:
L. Cueto-Felgueroso,
luis.cueto@upm.es

Citation:
Cueto-Felgueroso, L., and R. Juanes (2016), A discrete-domain description of multiphase flow in porous media: Rugged energy landscapes and the origin of hysteresis, *Geophys. Res. Lett.*, *43*, doi:10.1002/2015GL067015.

Received 13 NOV 2015
Accepted 29 JAN 2016
Accepted article online 2 FEB 2016

A discrete-domain description of multiphase flow in porous media: Rugged energy landscapes and the origin of hysteresis

Luis Cueto-Felgueroso[1,2] and Ruben Juanes[2]

[1]Department of Civil Engineering: Hydraulics, Energy and the Environment, Technical University of Madrid (UPM), Madrid, Spain, [2]Department of Civil and Environmental Engineering, Massachusetts Institute of Technology, Cambridge, Massachusetts, USA

Abstract We propose a discrete-domain model to describe mesoscale (many pore) immiscible displacements in porous media. We conceptualize the porous medium and fluid system as a set of weakly connected multistable compartments. The overall properties of the system emerge from the small-scale compartment dynamics. Our model aims at capturing the rugged energy landscape of multiphase porous media systems, emphasizing the role of metastability and local equilibria in the origin of hysteresis. Under two-phase displacements, the system behaves hysteretically, but our description does not rely on past saturations, turning points, or drainage/imbibition labels. We characterize the connection between micrometastability and overall system behavior, and elucidate the different nature of pressure-controlled and rate-controlled immiscible displacements in porous media.

Immiscible flows in porous media involve a complex sequence of pore-scale events, from the smooth, reversible displacement of interfaces to abrupt interfacial reconfigurations and rapid pore invasion cascades [*Måløy et al.*, 1992; *Furuberg et al.*, 1996; *Aker et al.*, 2000; *Xu et al.*, 2008; *Moebius et al.*, 2012; *Moebius and Or*, 2012; *Berg et al.*, 2013; *Moebius and Or*, 2014; *Pak et al.*, 2015]. These events are broadly categorized as *isons*, or smooth and reversible displacements of one phase by another one under a continuous variation of pressure or saturation; and *rheons*, or abrupt displacements associated with the sudden reconfiguration of unstable interfaces [*Morrow*, 1970]. Discontinuous changes in pressure or saturation have been referred to as Haines jumps [*Haines*, 1930], and they emerge as a key mechanism to understand the origin of irreversibility, or *hysteresis*, in porous media flow [*Everett and Whitton*, 1952; *Everett and Smith*, 1954; *Enderby*, 1955; *Morrow*, 1970]. Hysteresis persists at the many-pore scale (a representative elementary volume, REV): the water retention or *capillary pressure function*, $P_c \equiv P_c(S)$, which relates the fluid pressure difference—the capillary pressure, P_c—to the volumetric fraction of one of the fluids—its *saturation*, S—during a displacement or sequence of displacements, is hysteretic [*Albers*, 2014].

The interpretation of hysteresis as a consequence of irreversible transitions and multistability is at the heart of early hysteresis models [*Everett and Whitton*, 1952; *Everett and Smith*, 1954; *Enderby*, 1955] and recent experiments [*Moebius and Or*, 2012], and indicates an inherently nonequilibrium behavior. For a given volume fraction of fluids occupying the pore space, many stable configurations and interfacial arrangements are possible [*Morrow*, 1970]. Multistability also suggests rugged energy landscapes: in the absence of strong fluctuations, porous media systems may remain pinned at local minima of the free energy [*Frauenfelder et al.*, 1991; *Stillinger*, 1995; *Debenedetti and Stillinger*, 2001; *Wales*, 2001; *Gruebele*, 2002; *Stillinger and Debenedetti*, 2013].

We propose a mesoscale (REV) description of multiphase porous media flow that inherits fundamental features of pore-scale displacements—path dependence and "bursty" behavior. In the classical domain model of hysteresis [*Everett and Whitton*, 1952; *Everett and Smith*, 1954; *Enderby*, 1955], soil pores are bistable compartments—wet or dry—and the state of a pore is defined by its drying and wetting pressures. Hysteretic pressure-saturation diagrams are characterized, in the limit of many pores, by a distribution function quantifying the ratio of transitions from wet to dry over a certain pressure range [*Enderby*, 1956; *Poulovassillis*, 1962; *Poulovassillis and Childs*, 1971; *Topp*, 1971; *Mualem*, 1974]. Our framework shares with classical domain models the conceptual picture of a porous medium as a set of multistable units, interpreting

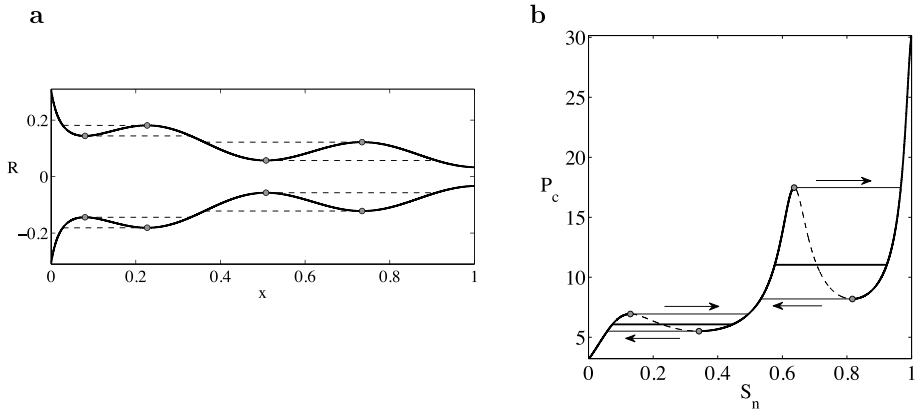

Figure 1. (a) A nonuniform capillary tube exhibits multiple stable configurations and hysteresis in two-phase displacements. A drainage experiment begins with the tube filled with the wetting fluid. By increasing the pressure of the nonwetting fluid at the inlet (left boundary), the meniscus separating the two fluids will advance inside the tube. We assume that the pressure drop across the interface—capillary pressure—can be calculated locally through the Young-Laplace equation. (b) The regions of decreasing capillary pressure (dashed lines) are unstable. At the end of a metastable branch, the meniscus advance will be discontinuous.

hysteresis as the result of a cascade of irreversible transitions among metastable states, but depart from the classical models in that it explicitly characterizes the *discrete* dynamics of the domains via a thermodynamic description.

The study of hysteresis as a nonequilibrium process has allowed in recent years to understand a wide range of physical and chemical systems, including adsorption [*Kierlik et al.*, 2001; *Bazant and Bazant*, 2012; *Bousquet et al.*, 2012], batteries [*Dreyer et al.*, 2010; *Bazant*, 2013], supercooled liquids and glass transitions [*Stillinger*, 1995; *Debenedetti and Stillinger*, 2001; *Stillinger and Debenedetti*, 2013; *Charbonneau et al.*, 2013], protein folding [*Frauenfelder et al.*, 1991; *Wales*, 2001; *Gruebele*, 2002; *Wales*, 2010], and epitaxial growth [*Chui and Weeks*, 1978; *Huse*, 1984; *Otto et al.*, 2004]. Our mathematical description builds on recent work characterizing the collective behavior of discrete sets of interconnected bistable units, from elastic chains [*Puglisi and Truskinovsky*, 2000, 2002], rate-independent plasticity [*Puglisi and Truskinovsky*, 2005], and carbon nanotube foams [*Fraternali et al.*, 2011], to hysteresis in insertion batteries [*Dreyer et al.*, 2010, 2011; *Sasaki et al.*, 2013], force-extension curves of modular biomolecules [*Prados et al.*, 2013; *Bonilla et al.*, 2015], and interconnected rubber balloons [*Moskon et al.*, 2013].

Multistability in immiscible displacements can be understood from a capillary tube whose diameter varies with axial position (Figure 1). The tube is connected on the left side to a reservoir containing nonwetting phase (*n*) and on the right to a reservoir containing wetting phase (*w*). The capillary pressure, $P_c = p_n - p_w$, determines the position of the meniscus, in accordance with the Young-Laplace equation. The state variable is the nonwetting-phase saturation S_n, which is the fraction of the tube volume filled with the nonwetting fluid. A sequence of increasing P_c will push the interface through locations of decreasing radius, until a section is reached where the tube radius increases again. Any further increase in P_c shifts the interface to a location compatible with the imposed pressure: intermediate positions are unstable. These interface jumps due to unstable configurations—Haines jumps—lead to abrupt changes in saturation and to hysteresis.

This conceptual picture of a capillary tube with nonmonotonic pressure-saturation relationship is the basis for our model. We describe a representative volume of porous medium as a *discrete* set of compartments or domains, $i = 1, \ldots, N$, and analyze fluid displacements as the collective process of filling and drying of these compartments. The pressure-saturation relationships for the individual compartments exhibit multistability, much like that of a nonuniform capillary tube with variable radius. The state of each compartment *i* is determined by its degree of saturation, s_i, and the total volume of wetting fluid in the system, V_w, is given by the averaged compartment volumes, $V_w = VS_w = \sum_{i=1}^{N} V_i s_i$, where S_w is the total wetting-phase saturation of the porous sample, V the total volume of pore space, and V_i the individual compartment volumes. We assume that the domains are weakly coupled, through a common imposed external field—the capillary pressure—or through a fixed saturation or injection rate constraint. We thus consider two distinct displacement protocols: either *pressure-controlled* or *saturation-controlled* conditions. In the former, the porous sample is subject to

prescribed pressures of the wetting and nonwetting phases, and the corresponding saturation is measured once the system has relaxed to an apparent equilibrium. In the latter, the wetting/nonwetting fluid is injected or withdrawn at a constant rate.

We characterize the multicompartment model dynamics through energy minimization arguments. Under prescribed pressure conditions, the relevant potential is a Gibbs-like free energy, while for saturation-controlled experiments, the evolution to equilibrium is driven by the minimization of a Helmholtz-like free energy. In the latter, the capillary pressure is no longer a given function of time but a Lagrange multiplier that is calculated by imposing the volume constraint. We assume that the free energy density of each compartment, f_i, depends only on its degree of saturation, $f_i \equiv f_i(s_i)$ [*Enderby*, 1955; *Puglisi and Truskinovsky*, 2000, 2002; *Dreyer et al.*, 2011; *Bonilla et al.*, 2015] and write the total free energy density of the system, F, as the sum of the individual ones, $F = \sum_{i=1}^{N} V_i f_i(s_i)$. Under isothermal conditions, and assuming incompressible fluids, this function models contributions from interfacial energies. If we interpret this energy as a Helmholtz free energy, then it must hold that the capillary pressure is minus the derivative of the free energy with respect to water volume, $P_c = -\frac{\partial F}{\partial V_w}$ [*Enderby*, 1955; *Morrow*, 1970; *Hassanizadeh and Gray*, 1993]. We also define a Gibbs-like energy potential,

$$G = F + P_c V_w = \sum_{i=1}^{N} V_i f_i(s_i) + P_c V_w, \tag{1}$$

whose minimization determines the route to equilibrium under constant-pressure experimental conditions [*Morrow*, 1970; *Bonilla et al.*, 2015]. The above total Gibbs free energy can be expressed in terms of the compartment free energy densities, g_i, as $G = \sum_{i=1}^{N} V_i g_i$, where $g_i = f_i + P_c s_i$. For simplicity, we assume in the following that all compartments represent equal pore volumes, $V_i = V_j, \forall i, j = 1, \dots, N$, and therefore, the global saturation is just the arithmetic mean, $S_w = \frac{1}{N}\sum s_i$. To incorporate multistability at the compartment level, we consider free energies f_i that have several disjoint convex regions, and therefore multiple local minima in g_i as P_c changes. Stable and *metastable* states are defined by the convexity of the free energy, $\frac{\partial^2 f_i}{\partial s_i^2} > 0$, while *unstable* regions are those intervals where f_i is concave. Stable and metastable equilibria become a local minimum of the Gibbs free energy for some value of the capillary pressure. Unstable states are unphysical: crossing an inflection point triggers a saturation jump toward another region of metastability in fixed-pressure displacements. Simple Leverett scaling [*Leverett*, 1941] of the compartment free energy densities suggests $f_i = \frac{\gamma \cos\theta}{r} f_i^*(s_i)$, where γ is the fluid-fluid surface tension, θ is the static contact angle, and $r = \sqrt{k/\phi}$ is a macroscopic estimate of the domain pore radius, where k is the permeability of the medium and ϕ its porosity.

Given the current conditions (capillary pressure P_c and the set of compartment saturations $\{s_1, \dots, s_N\}$), an imposed change in capillary pressure or saturation drives the system out of equilibrium, and the compartment saturations and/or pressures will change accordingly. We assume that the microscopic dynamics is a gradient flow, where compartment saturations evolve with steepest descent toward the minimization of the relevant energy potential. For the *fixed pressure* experiment, such potential is the total Gibbs free energy, G, and the dynamics reduces to the evolution equations

$$\eta \frac{\partial s_i}{\partial t} = -\frac{\partial G}{\partial s_i}, \quad \forall i = 1, \dots, N. \tag{2}$$

Since compartment energies depend on the local saturation alone, so that $\frac{\partial g_i}{\partial s_j} = 0, \forall j \neq i$, the above system can be written as

$$\frac{\eta}{V_i}\frac{\partial s_i}{\partial t} = -\frac{\partial g_i}{\partial s_i} = -\frac{\partial f_i}{\partial s_i} - P_c, \quad \forall i = 1, \dots, N. \tag{3}$$

In the present study we focus on deterministic dynamics and steady state saturations, and thus, the characteristic relaxation parameter η does not play any role. Compartment saturations s_i may relax toward local minima of g_i, fully sweeping metastable regions. This maximum delay strategy [*Puglisi and Truskinovsky*, 2005] provides the strongest hysteretic behavior and assumes that fluctuations and time scales are such that the system is unable to overcome energy barriers. Haines jumps are interpreted in this model as switching events among adjacent minima in a complex energy landscape [*Puglisi and Truskinovsky*, 2002, 2005;

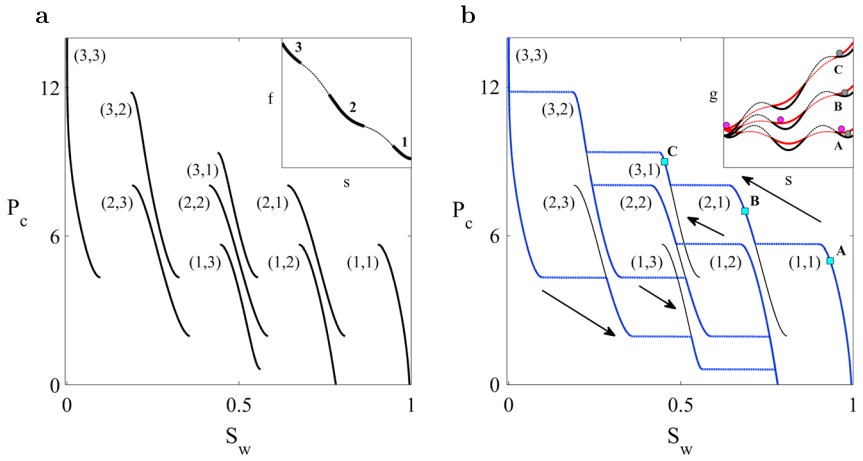

Figure 2. Hysteresis in pressure-controlled displacements. (a) Metastable branches for a two-compartment, three-well system. (b) We simulate two cycles of drainage and imbibition, illustrating the hysteretic behavior of the system. As we increase or decrease the capillary pressure, the P_c-S_w state follows reversible paths along metastable branches and jumps irreversibly among neighbor branches (blue line). (inset) For a given capillary pressure, compartment saturations relax toward minima of equation (3). A point in the P_c-S_w diagram is a combination of local equilibria at the compartments.

Dreyer et al., 2010, 2011]. The above Langevin equations (3) are also valid in the *fixed saturation* case, but in that case the capillary pressure is a Lagrange multiplier that enforces the constraint, $\frac{1}{N}\sum_{i=1}^{N} s_i = S_w$. This global coupling leads to long-range correlations and fluid redistribution among compartments.

In the examples presented hereafter, we adopt the following heuristic specification for the compartment specific free energies:

$$f_i^* = s_i \log(s_i) + (1 - s_i)\log(1 - s_i) - \omega_i s_i - c_i \cos(K\pi s_i), \tag{4}$$

where the first three terms yield a biased mixing rule describing a reversible wetting process. The coefficients ω_i can be identified as the strength of the wetting bias in the system and are proportional to the fluid-solid interfacial energy difference for a given compartment. In the present study, we assume for simplicity that they are constant, $\omega_i = \omega_0, \ \forall i = 1, \ldots, N$. The oscillatory term is a straightforward way to introduce energy barriers and break the energy function into disjoint convex regions. The coefficients $\mathbf{c} = \{c_1, c_2, \ldots, c_N\}$ define the characteristic height of the energy barriers, while K is the frequency of the oscillations (roughly the number of basins in the Gibbs-like energy). The overall model behavior can be illustrated with the simple case of a two-compartment system in the pressure-controlled setting (Figure 2). We set $N = 2$, $\omega_0 = 5$ and $K = 4$, and the coefficients defining the energy barriers are $c_1 = 0.2$ and $c_2 = 0.5$. Hence, both domains have three convex regions (Figure 2a, inset). Assuming that the two compartments represent the same pore volume, the total saturation is $S_w = \frac{1}{2}(s_1 + s_2)$.

We begin by reconstructing the equilibrium locus (Figure 2a). Compartment saturations must satisfy $P_c = -\frac{\partial f_i}{\partial s_i}$. Each of these equilibrium equations has up to three solutions, which lie inside convex regions of the free energy densities (Figure 2a, inset, plotted with solid lines). Taken individually, the compartment P_c-s_i diagrams comprise three disjoint metastable branches. Taken jointly, the full system P_c-S_w diagram (Figure 2a) comprises all possible combinations of compartment branches and is the locus of the states at which the system can be observed. We classify these branches with the pairs (m_1, m_2), indicating that the first compartment is in its m_1 region of metastability, while the second domain is in its m_2 region. Each point on a given branch represents a combination of local equilibria at the different compartments. Metastable branches are *isons*: they are reversible paths along which the system evolves continuously in the P_c-S_w space. Jumps among branches—*rheons*—occur when the current branch terminates, and the switching strategy determines the overall system dynamics. In the present maximum-delay paths, switching takes place among branches that differ by the state of one compartment. This one-by-one phase switching behavior is also observed in other physical systems composed of multistable units, such as elastic chains [*Puglisi and Truskinovsky*, 2000, 2002, 2005], insertion batteries [*Dreyer et al.*, 2010, 2011; *Sasaki et al.*, 2013], biomolecules [*Prados et al.*, 2013;

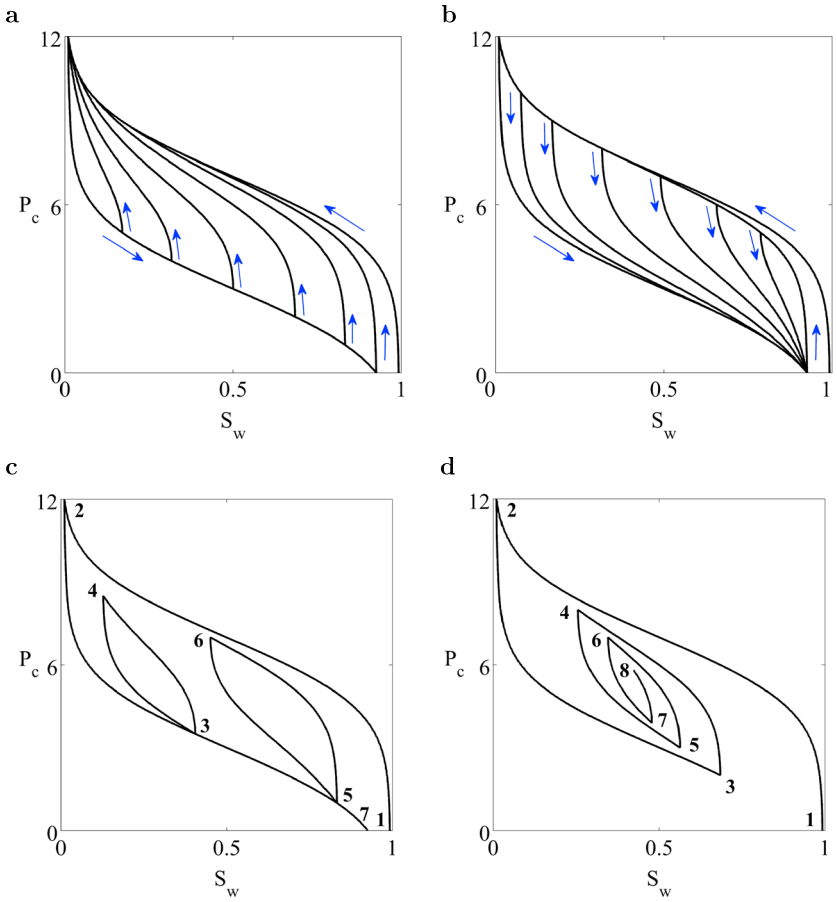

Figure 3. Pressure-saturation hysteresis diagram of a large system with $N = 17$ compartments and $K = 256$, with $\omega_0 = 5$ and barrier coefficients equally spaced between $c_1 = 10^{-4}$ and $c_{17} = 0.005$. (a) Primary drainage and main hysteresis loop with drainage scanning curves. (b) Primary drainage and main hysteresis loop with imbibition scanning curves. (c) Closed hysteresis loops. (d) Nested hysteresis cycles, illustrating the dense nature of the hysteresis diagram.

Bonilla et al., 2015], carbon nanotube foams [*Fraternali et al.*, 2011], or interconnected rubber balloons [*Dreyer et al.*, 2011; *Moskon et al.*, 2013].

In a constant-pressure experiment, we increase or decrease P_c according to a given protocol, letting saturations reach steady state after each pressure step. To simulate this type of cycles with our model (Figure 2b), we proceed as follows:

1. Initialize the system for a capillary pressure, e.g., $P_c = 0$: starting from initial compartment saturations near full saturation, $s_1 = s_2 = 0.99$, we relax the compartment saturations according to equation (3), to obtain, at $t \to \infty$, the equilibrium values that correspond to $P_c = 0$, $s_1(0)$, and $s_2(0)$. The overall water saturation is the average, $S_w = (s_1 + s_2)/2$.
2. Drainage/Imbibition cycles are simulated by repeating this equilibrium calculation for increasing/decreasing values of P_c, with pressure increments $\delta P_c = 0.01$. At each pressure step, the initial saturations are the steady state ones corresponding to the previous capillary pressure. When system fluctuations are neglected, individual compartment states can be trapped at the local minima of the Gibbs-like free energy, unable to overcome the energy barrier and cross toward the global minimum (Figure 2b, inset). At the end of the current branch, saturations jump to neighboring branches. At the microlevel, this event corresponds to the transition of one of the compartments to a neighbor basin (Figure 2b, inset).

Increasing the number of compartments and metastable branches per compartment leads to smaller-scale jumps and to smoother pressure-saturation curves (Figure 3). Many small Haines jumps do not imply, however, that hysteresis is negligible; on the contrary, a wide hysteresis region remains, as evidenced in Figure 3. The number of potential branches in the equilibrium locus increases very quickly with the number of

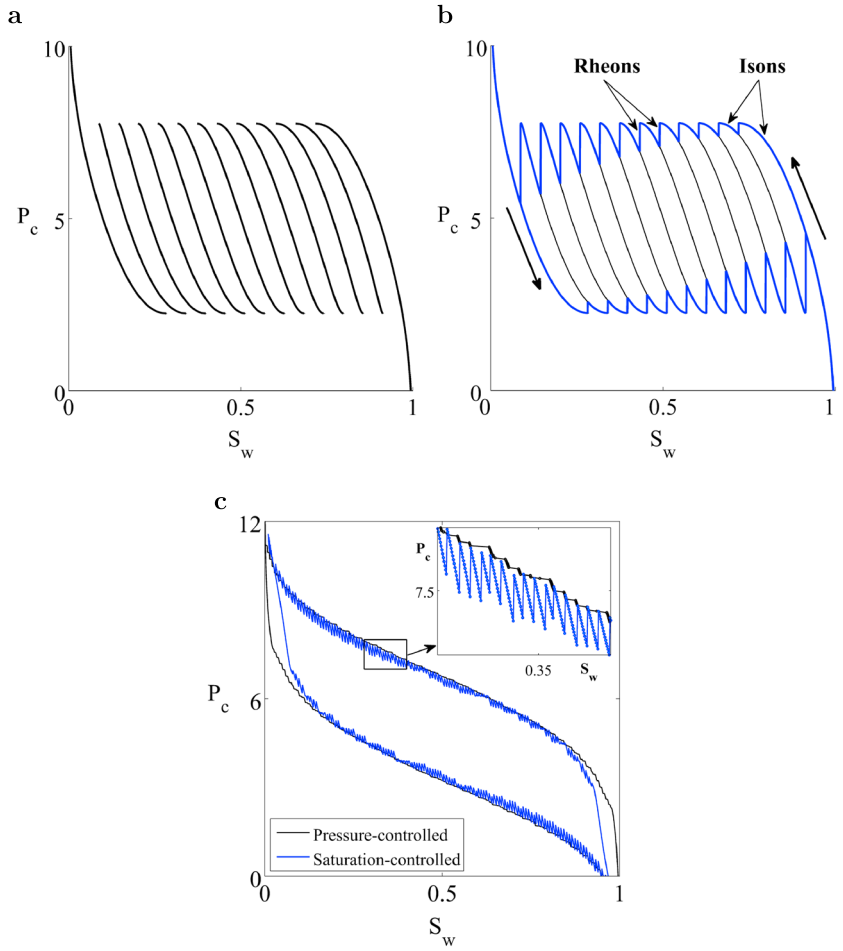

Figure 4. Overlapping branches and pressure jumps in saturation-controlled displacements. (a) The metastable branches overlap as the number of compartments increases. We model a system with $N = 12$ identical, bistable compartments, with $\omega_0 = 5$, $K = 2$, and $c_i = 0.6$, $\forall i = 1, \ldots, N$. (b) Sawtooth P_c-S_w behavior in a drainage-imbibition hysteresis loop (blue line). (c) A cycle of primary drainage and main imbibition, comparing the pressure-saturation diagrams for the pressure-controlled (black) and saturation-controlled (blue) conditions. The system comprises $N = 17$ compartments with $K = 8$, $\omega_0 = 5$, and barrier coefficients equally spaced between $c_1 = 0.005$ and $c_{17} = 0.155$.

compartments and local minima per compartment, resulting in a highly dense metastable region. This dense structure turns into smoothness of the scanning curves and to the commonly observed high-order scanning curves after many turning points and nested cycles [*Morrow and Harris*, 1965; *Morrow*, 1970] (Figure 3d).

One of the main features of our discrete-compartment model is the recognition of the difference between pressure-controlled and saturation-controlled conditions in multiphase displacements. The fundamental difference stems from the long-range interaction induced by the volume constraint. To illustrate this behavior, we begin with the simple case of a porous medium comprising $N = 12$ identical bistable compartments (Figure 4). The equilibrium locus of the overall system exhibits significant overlap (Figure 4a). We then simulate a full cycle of drainage and imbibition by imposing a decreasing saturation until $S_w = 0.01$ and then increasing the saturation until $S_w = 0.99$ (Figure 4b). The pressure-saturation diagram shows a characteristic sawtooth structure: the system evolves reversibly following individual branches, until the end of the branch triggers a jump toward a neighboring one. Pressure jumps are accompanied by fluid redistributions due to the global coupling. This phenomenon of pressure jumps and fluid redistribution has been characterized in experiments [*Crawford and Hoover*, 1966; *Furuberg et al.*, 1996; *Aker et al.*, 2000; *Xu et al.*, 2008; *Moebius and Or*, 2012; *Berg et al.*, 2013]. Finally, we compare the P_c-S_w diagrams for the pressure-controlled and saturation-controlled conditions for a system comprising $N = 17$ domains with $K = 8$, simulating a cycle of primary drainage and main imbibition (Figure 4c). The analysis based on the reconstruction of the equilibrium locus (Figure 4a)

explains why the system is still path dependent: the "bursty" behavior is associated with jumps among nearby metastable branches, but the density of branches is such that the amplitude of the hysteresis loop persists upon refinement.

The mechanistic description of mutiphase flow proposed here captures the nonequilibrium nature of pore-scale displacements. As a hysteresis model, our description has the remarkable property of being based on a unique characterization of the porous medium and fluid system, avoiding an explicit dependence on past saturations or drainage/imbibition labels. Being a thermodynamic model, it elucidates the different nature of fixed pressure and fixed volume—or fixed injection rate—displacements, potentially providing a link between pore-scale observations and large-scale processes. In this study we explored the fundamental idea that hysteresis in porous media flow is due to metastability, that is, to the fact that for given capillary pressure and saturation, many interfacial configurations are possible due to the complex structure of the pore space. Multistability suggests a rugged interfacial energy landscape. Our results suggest that even a simple characterization of such energy landscape can describe the complex behavior observed in hysteretic capillary equilibrium in porous media.

Acknowledgments
LCF gratefully acknowledges funding from the Spanish Ministry of Economy and Competitiveness (grants RyC-2012-11704 and CTM2014-54312-P).

References

Aker, E., K. Måløy, A. Hansen, and S. Basak (2000), Burst dynamics during drainage displacements in porous media: Simulations and experiments, *Europhys. Lett.*, *51*, 55–61.
Albers, B. (2014), Modeling the hysteretic behavior of the capillary pressure in partially saturated porous media: A review, *Acta Mech.*, *225*, 2163–2189.
Bazant, M. Z. (2013), Theory of chemical kinetics and charge transfer based on nonequilibrium thermodynamics, *Accounts Chem. Res.*, *46*, 1144–1160.
Bazant, M. Z., and Z. P. Bazant (2012), Theory of sorption hysteresis in nanoporous solids: Part II. Molecular condensation, *J. Mech. Phys. Solids*, *60*, 1660–1675.
Berg, S., et al. (2013), Real-time 3D imaging of Haines jumps in porous media flow, *Proc. Natl. Acad. Sci. U.S.A.*, *110*, 3755–3759.
Bonilla, L. L., A. Carpio, and A. Prados (2015), Theory of force-extension curves for modular proteins and DNA hairpins, *Phys. Rev. E*, *91*, 52712.
Bousquet, D., F.-X. Coudert, and A. Boutin (2012), Free energy landscapes for the thermodynamic understanding of adsorption-induced deformations and structural transitions in porous materials, *J. Chem. Phys.*, *137*, 44118.
Charbonneau, P., J. Kurchan, G. Parisi, P. Urbani, and F. Zamponi (2013), Fractal free energy landscapes in structural glasses, *Nat. Commun.*, *5*, 3725, doi:10.1038/ncomms4725.
Chui, S. T., and J. D. Weeks (1978), Dynamics of the roughening transition, *Phys. Rev. Lett.*, *40*, 733–736.
Crawford, F. W., and G. M. Hoover (1966), Flow of fluids through porous mediums, *J. Geoph. Res.*, *71*, 2911–2917.
Debenedetti, P. G., and F. H. Stillinger (2001), Supercooled liquids and the glass transition, *Nature*, *410*, 259–267.
Dreyer, W., J. Jamnik, C. Guhlke, R. Huth, J. Moškon, and M. Gaberšček (2010), The thermodynamic origin of hysteresis in insertion batteries, *Nat. Mater.*, *9*, 448–453.
Dreyer, W., C. Guhlke, and R. Huth (2011), The behavior of a many-particle electrode in a lithium-ion battery, *Phys. D*, *240*, 1008–1019.
Enderby, J. A. (1955), The domain model of hysteresis. Part 1.—Independent domains, *Trans. Faraday Soc.*, *51*, 835–848.
Enderby, J. A. (1956), The domain model of hysteresis. Part 2.—Interacting domains, *Trans. Faraday Soc.*, *52*, 406–420.
Everett, D. H., and F. W. Smith (1954), A general approach to hysteresis. Part 2. Development of the domain theory, *Trans. Faraday Soc.*, *50*, 187–197.
Everett, D. H., and W. I. Whitton (1952), A general approach to hysteresis, *Trans. Faraday Soc.*, *48*, 749–752.
Fraternali, F., T. Blesgen, A. Amendola, and C. Daraio (2011), Multiscale mass-spring models of carbon nanotube foams, *J. Mech. Phys. Solids*, *59*, 89–102.
Frauenfelder, H., S. G. Sligar, and P. G. Wolynes (1991), The energy landscapes and motions of proteins, *Science*, *254*, 1598–1603.
Furuberg, L., K. Måløy, and J. Feder (1996), Intermittent behavior in slow drainage, *Phys. Rev. E*, *53*, 966–977.
Gruebele, M. (2002), Protein folding: The free energy surface, *Curr. Opin. Struct. Biol.*, *12*, 161–168.
Haines, W. B. (1930), Studies in the physical properties of soil. V. The hysteresis effect in capillary properties, and the modes of moisture distribution associated therewith, *J. Agric. Sci.*, *20*, 97–116.
Hassanizadeh, S. M., and W. G. Gray (1993), Thermodynamic basis of capillary pressure in porous media, *Water Resour. Res.*, *29*, 3389–3405.
Huse, D. A. (1984), Renormalization-group analysis of layering transitions in solid films, *Phys. Rev. Lett.*, *30*, 1371–1376.
Kierlik, E., P. A. Monson, M. L. Rosinberg, L. Sarkisov, and G. Tarjus (2001), Capillary condensation in disordered porous materials: Hysteresis versus equilibrium behavior, *Phys. Rev. Lett.*, *87*, 55701.
Leverett, M. C. (1941), Capillary behavior in porous solids, *Trans. AIME*, *142*, 152–168.
Måløy, K., L. Furuberg, J. Feder, and Jø, T.ssang (1992), Dynamics of slow drainage in porous media, *Phys. Rev. Lett.*, *68*, 2161–2164.
Moebius, F., and D. Or (2012), Interfacial jumps and pressure bursts during fluid displacement in interacting irregular capillaries, *J. Colloid Interface Sci.*, *377*, 406–415.
Moebius, F., and D. Or (2014), Inertial forces affect fluid front displacement dynamics in a pore-throat network model, *Phys. Rev. E*, *90*, 23019.
Moebius, F., D. Canone, and D. Or (2012), Characteristics of acoustic emissions induced by fluid front displacement in porous media, *Water Resour. Res.*, *48*, W11507, doi:10.1029/2012WR012525.
Morrow, N. R. (1970), Physics and thermodynamics of capillary action in porous media, *Ind. Eng. Chem. Res.*, *62*, 32–56.
Morrow, N. R., and C. C. Harris (1965), Capillary equilibrium in porous materials, *Soc. Pet. Eng. J.*, *5*, 15–24.
Moskon, J., J. Jamnik, and M. Gaberscek (2013), In depth discussion of selected phenomena associated with intrinsic battery hysteresis: Battery electrode versus rubber balloons, *Solid State Ionics*, *238*, 24–29.
Mualem, Y. (1974), A conceptual model of hysteresis, *Water Resour. Res.*, *10*, 514–520.
Otto, F., P. Penzlera, A. Rätz, T. Rump, and A. Voigt (2004), A diffuse-interface approximation for step flow in epitaxial growth, *Nonlinearity*, *17*, 477–491.

Pak, T., I. B. Butler, S. Geiger, M. I. J. van Dijke, and K. S. Sorbie (2015), Droplet fragmentation: 3D imaging of a previously unidentified pore-scale process during multiphase flow in porous media, *Proc. Natl. Acad. Sci. U.S.A.*, *112*, 1947–1952.
Poulovassillis, A. (1962), Hysteresis of pore water, an application of the concept of independent domains, *Soil Sci.*, *93*, 405–412.
Poulovassillis, A., and E. C. Childs (1971), The hysteresis of pore water: The non-independence of domains, *Soil Sci.*, *112*, 301–312.
Prados, A., A. Carpio, and L. L. Bonilla (2013), Sawtooth patterns in force-extension curves of biomolecules: An equilibrium-statistical-mechanics theory, *Phys. Rev. E*, *88*, 12704.
Puglisi, G., and L. Truskinovsky (2000), Mechanics of a discrete chain with bi-stable elements, *J. Mech. Phys. Solids*, *48*, 1–27.
Puglisi, G., and L. Truskinovsky (2002), Rate independent hysteresis in a bi-stable chain, *J. Mech. Phys. Solids*, *50*, 165–187.
Puglisi, G., and L. Truskinovsky (2005), Thermodynamics of rate-independent plasticity, *J. Mech. Phys. Solids*, *53*, 655–679.
Sasaki, T., Y. Ukyo, and P. Novák (2013), Memory effect in a lithium-ion battery, *Nat. Mater.*, *12*, 569–575.
Stillinger, F. H. (1995), A topographic view of supercooled liquids and glass formation, *Science*, *267*, 1935–1939.
Stillinger, F. H., and P. G. Debenedetti (2013), Glass transition thermodynamics and kinetics, *Annu. Rev. Condens. Matter Phys.*, *4*, 263–285.
Topp, G. C. (1971), Soil water hysteresis in silt loam and clay loam soils, *Water Resour. Res.*, *7*, 914–920.
Wales, D. J. (2001), A microscopic basis for the global appearance of energy landscapes, *Science*, *293*, 2067–2070.
Wales, D. J. (2010), Energy landscapes: Some new horizons, *Curr. Opin. Struct. Biol.*, *20*, 3–10.
Xu, L., S. Davies, A. Schofield, and D. Weitz (2008), Dynamics of drying in 3D porous media, *Phys. Rev. Lett.*, *101*, 94502.